Optimal Second-Harmonic Current Injection for Capacitor Voltage Fluctuation Reduction in Hybrid MMCs Under Grid-side SLG Faults

Jianzhong Xu, *Senior Member*, *IEEE*, Weicheng Deng, Gen Li*, *Member*, *IEEE*, Chengyong Zhao*, *Senior Member*, *IEEE*, and Chongru Liu, *Senior Member*, *IEEE*

Abstract — **The second-harmonic injection strategy for modular multilevel converters (MMCs) can effectively suppress the capacitor voltage fluctuation in steady states. However, the capacitor voltage fluctuation under grid-side single-line-to-ground (SLG) faults will be more severe. Moreover, there is no research on the mitigation of capacitor voltage fluctuation under grid-side SLG faults for the hybrid MMC with mixed half-bridge and full-bridge sub-modules. To address this issue for hybrid MMCs, an optimal second-harmonic current injection scheme for mitigating the capacitor voltage fluctuation in the hybrid MMC under grid-side SLG faults is proposed in this paper. The mathematical models of arm power fluctuations of the hybrid MMC are firstly developed under both steady states and grid-side SLG faults. Then, the principle and optimal strategy of the proposed capacitor voltage fluctuation strategy are presented. The capacitor voltage fluctuation under grid-side SLG faults can be reduced by suppressing the three-phase arm power fluctuations. A hybrid MMC model with the proposed scheme has been established in PSCAD/EMTDC to verify its effectiveness and feasibility. Simulation results show that the average voltage fluctuation reduction rate can reach 55.77% with the proposed strategy.**

Index Terms — **Second-harmonic current injection; hybrid MMC; HB and FB submodule; grid-side SLG faults; voltage fluctuation.**

I. INTRODUCTION

Modular multilevel converter (MMC) has attracted more attention compared to line commutated converter (LCC) for high-voltage direct-current (HVDC) transmission, due to their advantages of low harmonics, flexible control, modularity and no commutation failure [1], [2]. At present, MMCs have been widely used in high voltage and large capacity scenarios [3], [4]. However, the high volume/weight and cost of MMC-HVDC are still the concerns of manufacturers and market players. Submodule (SM) capacitors of an MMC account for about 1/2 of its volume [5], [6]. Therefore, it is

necessary to reduce the capacitance of SM capacitors so as to reduce the overall volume/weight and cost of the MMC.

The capacitance can be reduced if the fluctuations of SM capacitor voltages can be regulated within a minimum range. SM voltage fluctuation suppression schemes of half-bridge (HB) MMC have been widely investigated in the open literature. In [7], a circulating current elimination method has been proposed to reduce the HB-SM voltage fluctuation. It has been found in [8] that the capacitor voltage ripple can be further reduced by injecting a second-harmonic circulating current properly. Based on [8], an optimal design of the injected second-harmonic circulating current is carried out in [9]. In [10] and [11], mathematical models of the capacitor voltage fluctuation and energy storage requirements for HB-MMC have been developed. Reference [12] investigates how to reduce the capacitor voltage fluctuation using a third-harmonic voltage injection. The above methods all contribute to reducing the SM voltage fluctuation of HB-MMC.

It is known that the HB-MMC does not have DC fault blocking capability like the full-bridge (FB) MMC [13]-[14]. However, the FB-MMC exhibits the challenges of their high capital cost and power losses. The HB-SM and FB-SM based hybrid MMC combines the merits of the two types of MMCs [15]-[16]: 1) The hybrid MMC has DC fault-ride-through capability; 2) The hybrid MMC has a wider modulation index range compared to HB-MMC, which provides more space to improve the suppression of capacitor voltage fluctuation. Under steady states, the modulation index of 1.414 can significantly reduce the fundamental frequency component of the SM capacitor voltage, and at the same time, suppress the fluctuation of the SM capacitor voltage [19], [20]. In [19], an optimal second-harmonic current injection of amplitude and phase has been developed based on the defined fluctuation function of SM capacitor voltage. An optimal circulating current injection method considering the limitation of the current rating of semiconductor (switch) has been studied in [20]. In addition, the hybrid MMC may experience unipolar arm currents under reduced DC voltage conditions, which will affect the charge/discharge balance of HB-SM capacitors in each fundamental cycle [21]-[23]. A second-harmonic circulating current injection to achieve arm currents in hybrid MMC bipolar during reduced DC voltage conditions has been proposed in [23]. However, the objective of [23] is not to

investigate the control of MMC under SLG faults but to achieve maximum power transfer under a reduced DC voltage, in which case the AC side voltages are not affected by any faults.

However, the abovementioned work only analyzes the harmonic injection method under steady states. The impact of hybrid MMC's grid-side unbalanced faults on the capacitor voltage fluctuation suppression schemes has been underresearched. It is well known that the single-line-to-ground (SLG) fault is one of the most common faults in power systems. The modeling and control of HB-MMC subject to grid-side SLG faults have been investigated in [24]. Following [19], [25] further investigates the impact of FB-MMC's modulation index on the SM capacitor voltage fluctuation under SLG faults. However, the above studies have not considered the impact of SLG faults on the harmonic current injection strategy which is one of the most important methods to suppress capacitor voltage fluctuation. Moreover, these methods do not apply to the hybrid MMC because of its special converter configuration of mixed HB- and FB-SMs. A dual harmonic current injection strategy for reducing the SM voltage fluctuation in hybrid MMCs has been proposed in [26]. However, the work mainly focuses on SM voltage fluctuation mitigation under steady-state operation. Although tests under grid-side SLG faults have been conducted, there is no further theoretical analysis and optimal design of the harmonic current injection for the SM voltage fluctuation under SLG faults.

This paper aims to address the abovementioned issues. The main contributions of this work include: 1) Theoretically analyze the impact of converter grid-side SLG faults on the second-harmonic injection strategy in the hybrid MMC; 2) Develop mathematical models of the arm power fluctuation under both steady states and grid-side SLG faults; 3) Propose an optimal second-harmonic current injection scheme to minimize arm power ripples and therefore, reduce the SM voltage fluctuation under grid-side SLG fault conditions. The studies reveal that, under grid-side SLG faults, the SM voltage fluctuation with the second-harmonic current injection strategy will be larger than that without the injection strategy. This means that the second-harmonic current injection strategy brings negative effects on the hybrid MMC under grid-side SLG faults. The analysis is verified in PSCAD/EMTDC. Simulation results indicate that the SM capacitor voltage fluctuation under an SLG fault can be effectively mitigated by the proposed second-harmonic current injection scheme. In addition, the accuracy of the proposed mathematical models of the arm power model is high.

II. MODELING OF ARM POWER FLUCTUATION IN HYBRID MMCS

A. Structure and Arm Power Fluctuation of Hybrid MMCs

Fig. 1 gives the structure of hybrid MMCs, which consists of six arms. Each arm consists of N SMs, including n HB-SMs and m FB-SMs. U_{dc} is the DC voltage, I_{dc} is the DC current, u_a, u_b and u_c are the AC voltages and L_{arm} is the arm inductor.
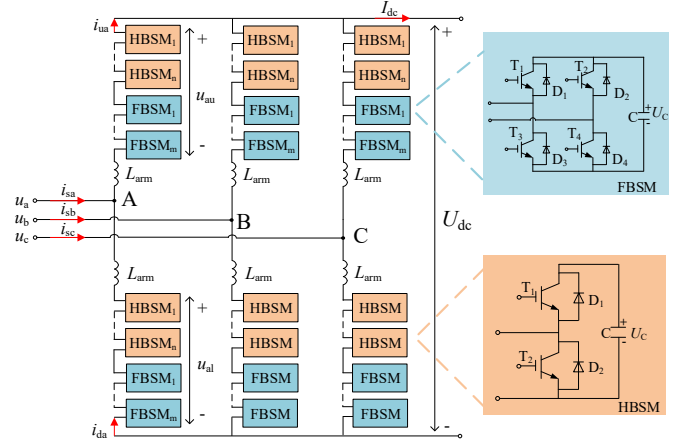

Fig. 1. Structure of a hybrid MMC.

As the three-phase arm power fluctuations are symmetrical under steady states, phase A is taken as an example. The positive directions of the voltage and current are defined in Fig. 1. Then, the voltages u_{au} and u_{al} across the upper and lower arms can be expressed as:

$$\begin{cases} u_{au} = \dfrac{1}{2}U_{dc}(1 - m\sin\omega t) \\ u_{al} = \dfrac{1}{2}U_{dc}(1 + m\sin\omega t) \end{cases}, \quad (1)$$

where ω is the fundamental angular frequency. m is the modulation index of the hybrid MMC, which can be expressed as:

$$m = \frac{2U_{ac}}{U_{dc}}, \quad (2)$$

where U_{ac} is the amplitude of AC voltage. Considering the second-harmonic circulating current, the upper and lower arm currents i_{au} and i_{al} can be expressed as:

$$\begin{cases} i_{au} = \dfrac{1}{2}I_m(\dfrac{1}{2}m\cos\varphi_1 + \sin(\omega t - \varphi_1) + k_2\sin(2\omega t + \varphi_2)) \\ i_{al} = \dfrac{1}{2}I_m(\dfrac{1}{2}m\cos\varphi_1 - \sin(\omega t - \varphi_1) + k_2\sin(2\omega t + \varphi_2)) \end{cases}, \quad (3)$$

where φ_1 is the power factor angle, I_m is the amplitude of AC current and φ_2 is the initial phase angle of the second-harmonic circulating current. k_2 is the second-harmonic injection coefficient which is calculated by $2I_2/I_m$ and I_2 is the amplitude of the second-harmonic circulating current.

The instantaneous arm power can be obtained by substituting (1) and (3) into the following expression:

$$\begin{cases} P_{au} = u_{au} \times i_{au} \\ P_{al} = u_{al} \times i_{al} \end{cases}, \quad (4)$$

i.e.,

$$\begin{cases} P_{au} = \dfrac{U_{dc}I_m}{4}(-\dfrac{1}{2}m^2\cos\varphi_1\sin\omega t + \sin(\omega t - \varphi_1) + \dfrac{1}{2}m\cos(2\omega t - \varphi_1) \\ \quad + k_2\sin(2\omega t + \varphi_2) + \dfrac{1}{2}mk_2\cos(3\omega t + \varphi_2) - \dfrac{1}{2}mk_2\cos(\omega t + \varphi_2)) \\ P_{al} = \dfrac{U_{dc}I_m}{4}(\dfrac{1}{2}m^2\cos\varphi\sin\omega t - \sin(\omega t - \varphi_1) + \dfrac{1}{2}m\cos(2\omega t - \varphi_1) \\ \quad + k_2\sin(2\omega t + \varphi_2) - \dfrac{1}{2}mk_2\cos(3\omega t + \varphi_2) + \dfrac{1}{2}mk_2\cos(\omega t + \varphi_2)) \end{cases}. \quad (5)$$

B. Mathematical Model of Arm Power Fluctuation under Grid-side SLG Faults

To block the zero-sequence current, the Y/Δ winding configuration is usually used for the converter interface transformer. Therefore, the AC voltages are only comprised of positive- and negative-sequence components. To suppress the negative-sequence current under grid-side faults, the negative-sequence double-closed loop controller is applied. Fig. 2 presents the control diagram of hybrid MMCs with the second-harmonic current injection.
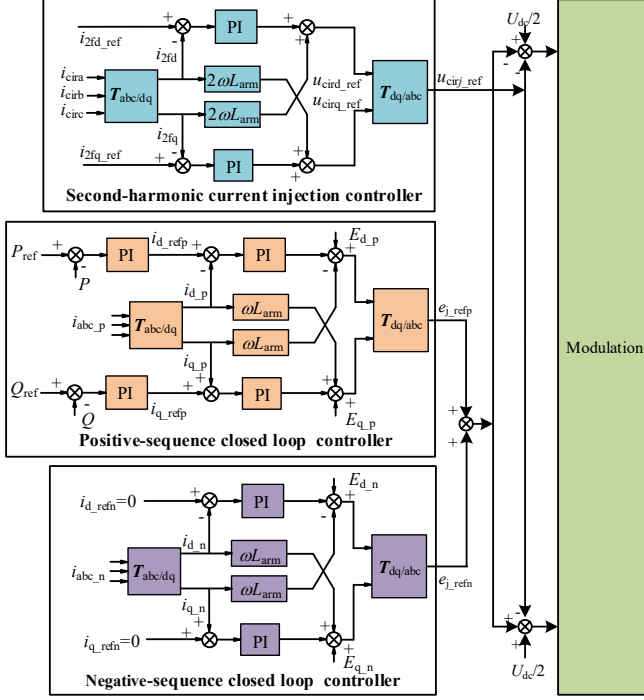

Fig. 2. Control diagram of hybrid MMCs with second-harmonic current injection.

The control system consists of two parts: the AC reference voltage controller and the second-harmonic current injection controller. The AC reference voltages controller includes positive- and negative-sequence closed loop controllers which are typical control in MMC[27]. i_{d_refp} and i_{q_refp} are the references of positive-sequence dq-axis currents, which generate the positive-sequence AC reference voltage e_{j_refp} ($j=a$, b, c) through dq inverse transformation. i_{d_refn} and i_{q_refn} are the references of negative-sequence dq-axis currents. e_{j_refn} is negative-sequence AC reference voltage. The second-harmonic current injection controller uses the references of the second-harmonic currents of dq-axis i_{2fd_ref} and i_{2fq_ref} to generate the reference of the common-mode voltage U_{cirj_ref}. It is noted that i_{2fd_ref} and i_{2fq_ref} are determined by the amplitude and phase of the injected second-harmonic circulating current.

This part takes a solid SLG fault in phase A as an example to analyze. After the fault, the positive- and negative-sequence AC voltages are:

$$\begin{cases} u_{as\_p} = \dfrac{2}{3}U_m\sin\omega t \\ u_{bs\_p} = \dfrac{2}{3}U_m\sin(\omega t - \dfrac{2}{3}\pi) \\ u_{cs\_p} = \dfrac{2}{3}U_m\sin\omega t(\omega t + \dfrac{2}{3}\pi) \end{cases}, \quad (6)$$

$$\begin{cases} u_{as\_n} = \dfrac{1}{3}U_m\sin(\omega t - \dfrac{2}{3}\pi) \\ u_{bs\_n} = \dfrac{1}{3}U_m\sin\omega t \\ u_{cs\_n} = \dfrac{1}{3}U_m\sin(\omega t + \dfrac{2}{3}\pi) \end{cases}. \quad (7)$$

According to (6) and (7), the three-phase upper arm voltages can be obtained:

$$\begin{cases} u_{au\_f} = \dfrac{1}{2}U_{dc} - \dfrac{2}{3}U_m\sin\omega t - \dfrac{1}{3}U_m\sin(\omega t - \dfrac{2}{3}\pi) \\ u_{bu\_f} = \dfrac{1}{2}U_{dc} - \dfrac{2}{3}U_m\sin(\omega t - \dfrac{2}{3}\pi) - \dfrac{1}{3}U_m\sin\omega t \\ u_{cu\_f} = \dfrac{1}{2}U_{dc} - U_m\sin\omega t(\omega t + \dfrac{2}{3}\pi) \end{cases}. \quad (8)$$

To avoid overcurrent during the fault, the transmission power will be reduced to two-thirds of the rated power. Then, the upper arm currents can be expressed as:

$$\begin{cases} i_{au\_f} = (\dfrac{1}{2} + \dfrac{\sqrt{3}}{6}\tan\varphi_1)\dfrac{1}{4}mI_m\cos\varphi_1 + \dfrac{1}{2}I_m\sin(\omega t - \varphi_1) \\ \quad + I_2\sin(2\omega t + \varphi_2) \\ i_{bu\_f} = (\dfrac{1}{2} - \dfrac{\sqrt{3}}{6}\tan\varphi_1)\dfrac{1}{4}mI_m\cos\varphi_1 + \dfrac{1}{2}I_m\sin\left(\omega t - \varphi_1 - \dfrac{2}{3}\pi\right) \\ \quad + I_2\sin(2\omega t + \varphi_2 + \dfrac{2}{3}\pi) \\ i_{cu\_f} = \dfrac{1}{4}mI_m\cos\varphi_1 + \dfrac{1}{2}I_m\sin\left(\omega t - \varphi_1 + \dfrac{2}{3}\pi\right) \\ \quad + I_2\sin(2\omega t + \varphi_2 - \dfrac{2}{3}\pi) \end{cases}. \quad (9)$$

Substituting (8) and (9) into (5), the upper arm power can be obtained:

$$\begin{cases}
P_{\text{au\_f}} = \dfrac{U_{\text{dc}}I_{\text{m}}}{4}(-\dfrac{1}{3}(\dfrac{1}{2}+\dfrac{\sqrt{3}}{6}\tan\varphi_1)m^2\cos\varphi_1\sin\omega t+\sin(\omega t-\varphi_1) \\
-\dfrac{1}{6}(\dfrac{1}{2}+\dfrac{\sqrt{3}}{6}\tan\varphi_1)m^2\cos\varphi_1\sin(\omega t-\dfrac{2}{3}\pi) \\
-\dfrac{1}{3}mk_2\cos(\omega t+\varphi_2)-\dfrac{1}{6}mk_2\cos(\omega t+\varphi_2+\dfrac{2}{3}\pi) \\
+k_2\sin(2\omega t+\varphi_2)+\dfrac{1}{3}m\cos(2\omega t-\varphi_1)+\dfrac{1}{3}mk_2\cos(3\omega t+\varphi_2) \\
+\dfrac{1}{6}m\cos(2\omega t-\varphi_1-\dfrac{2}{3}\pi)+\dfrac{1}{6}mk_2\cos(3\omega t+\varphi_2-\dfrac{2}{3}\pi)) \\
P_{\text{bu\_f}} = \dfrac{U_{\text{dc}}I_{\text{m}}}{4}(-\dfrac{1}{3}k_2m\cos(\omega t+\varphi_2-\dfrac{2}{3}\pi) \\
-\dfrac{1}{3}(\dfrac{1}{2}-\dfrac{\sqrt{3}}{6}\tan\varphi_1)m^2\cos\varphi_1\sin(\omega t-\dfrac{2}{3}\pi) \\
-\dfrac{1}{6}(\dfrac{1}{2}-\dfrac{\sqrt{3}}{6}\tan\varphi_1)m^2\cos\varphi_1\sin\omega t+\sin(\omega t-\varphi_1-\dfrac{2}{3}\pi) \\
-\dfrac{1}{6}mk_2\cos(\omega t+\varphi_2+\dfrac{2}{3}\pi)+\dfrac{1}{3}m\cos(2\omega t-\varphi_1+\dfrac{2}{3}\pi) \\
+\dfrac{1}{6}m\cos(2\omega t-\varphi_1-\dfrac{2}{3}\pi)+k_2\sin(2\omega t+\varphi_2+\dfrac{2}{3}\pi) \\
+\dfrac{1}{3}mk_2\cos(3\omega t+\varphi_2)+\dfrac{1}{6}mk_2\cos(3\omega t+\varphi_2+\dfrac{2}{3}\pi)) \\
P_{\text{cu\_f}} = \dfrac{U_{\text{dc}}I_{\text{m}}}{4}(-\dfrac{1}{2}m^2\cos\varphi_1\sin(\omega t+\dfrac{2}{3}\pi)+\sin(\omega t-\varphi_1+\dfrac{2}{3}\pi) \\
+\dfrac{1}{2}m\cos(2\omega t-\varphi_1+\dfrac{4}{3}\pi)+k_2\sin(2\omega t+\varphi_2+\dfrac{4}{3}\pi) \\
+\dfrac{1}{2}mk_2\cos(3\omega t+\varphi_2)-\dfrac{1}{2}mk_2\cos(\omega t+\varphi_2+\dfrac{2}{3}\pi))
\end{cases} \quad .(10)$$

It can be observed from (5) and (10) that the power fluctuation of phase C remains constant as pre-fault and the power fluctuations of phases A and B are quite different from the pre-fault state.

C. SM Voltage Behavior under SLG Faults

In this section, it is proved through simulation that the second-harmonic current injection strategy used for steady states will increase the capacitor voltage fluctuation under grid-side SLG faults. This part takes the steady state with $m=1$ and $\cos\varphi_1=0.8$ as an example to analyze. Fig. 3 presents the capacitor voltage fluctuation of hybrid MMC with the second-harmonic current injection strategy used for steady states.
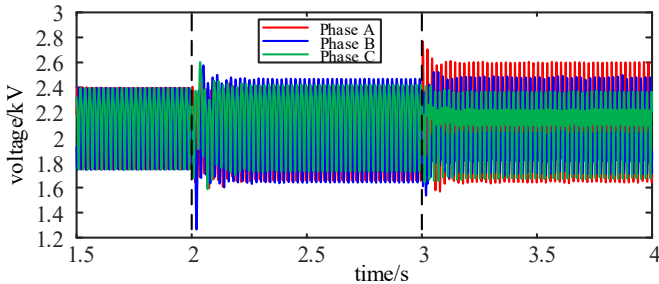

Fig. 3. Capacitor voltage fluctuation of hybrid MMC with the second-harmonic current injection strategy used for steady states.

Before $t=2.0$ s, the system is in the steady state. The SLG fault occurs at $t=2.0$ s. Before $t=3.0$ s, the circulating current

elimination method in [7] is applied. Then, after $t=3.0$ s, the second-harmonic current injection scheme proposed in [19] is activated. It can be seen that, after $t=3.0$ s, the capacitor voltage fluctuation becomes severer, which may damage the semiconductor devices and capacitors.

III. PROPOSED OPTIMAL SECOND-HARMONIC CURRENT INJECTION SCHEME

The arm power fluctuation changes along with the capacitor voltage ripples. A large voltage ripple would lead to a large arm power fluctuation. The fundamental-frequency and second-harmonic components are dominating the three-phase arm power fluctuations, which will be derived in this section. Based on this, an optimal second-harmonic current injection strategy in hybrid MMCs under SLG Faults is proposed to suppress the three-phase arm power fluctuation.

A. Extraction of the Amplitude of Arm Power Fluctuation

From equation (10), the fundamental-frequency and second-harmonic components $P_{\text{au\_f1}}$ and $P_{\text{au\_f2}}$ of the upper arm power fluctuation in phase A can be obtained:

$$\begin{cases}
P_{\text{au\_f1}} = \dfrac{U_{\text{dc}}I_{\text{m}}}{4}[-\dfrac{1}{3}(\dfrac{1}{2}+\dfrac{\sqrt{3}}{6}\tan\varphi_1)m^2\cos\varphi_1\sin\omega t \\
-\dfrac{1}{6}(\dfrac{1}{2}+\dfrac{\sqrt{3}}{6}\tan\varphi_1)m^2\cos\varphi_1\sin(\omega t-\dfrac{2}{3}\pi)-\dfrac{1}{3}mk_2\cos(\omega t+\varphi_2) \\
-\dfrac{1}{6}mk_2\cos(\omega t+\varphi_2+\dfrac{2}{3}\pi)+\sin(\omega t-\varphi_1)] \\
P_{\text{au\_f2}} = \dfrac{U_{\text{dc}}I_{\text{m}}}{4}[k_2\sin(2\omega t+\varphi_2)+\dfrac{1}{3}m\cos(2\omega t-\varphi_1) \\
+\dfrac{1}{6}m\cos(2\omega t-\varphi_1-\dfrac{2}{3}\pi)]
\end{cases} \quad (11)$$

Using the trigonometric transformation, $P_{\text{au\_f1}}$ and $P_{\text{au\_f2}}$ can be rewritten as:

$$P_{\text{au\_f1}} = A_{\text{au\_f1}}\sin\omega t + B_{\text{au\_f1}}\cos\omega t$$

$$\begin{cases}
A_{\text{au\_f1}} = \dfrac{U_{\text{dc}}I_{\text{m}}}{4}[(-\dfrac{1}{4}(\dfrac{1}{2}+\dfrac{\sqrt{3}}{6}\tan\varphi_1)m^2+1)\cos\varphi_1 \\
+\dfrac{1}{4}mk_2\sin\varphi_2+\dfrac{\sqrt{3}}{12}mk_2\cos\varphi_2] \\
B_{\text{au\_f1}} = \dfrac{U_{\text{dc}}I_{\text{m}}}{4}[\dfrac{\sqrt{3}}{12}(\dfrac{1}{2}+\dfrac{\sqrt{3}}{6}\tan\varphi_1)m^2\cos\varphi_1-\sin\varphi_1 \\
-\dfrac{1}{4}mk_2\cos\varphi_2+\dfrac{\sqrt{3}}{12}mk_2\sin\varphi_2]
\end{cases} \quad (12)$$

$$P_{\text{au\_f2}} = A_{\text{au\_f2}}\sin 2\omega t + B_{\text{au\_f2}}\cos 2\omega t$$

$$\begin{cases}
A_{\text{au\_f2}} = \dfrac{U_{\text{dc}}I_{\text{m}}}{4}[k_2\cos\varphi_2+\dfrac{1}{4}m\sin\varphi_1+\dfrac{\sqrt{3}}{12}m\cos\varphi_1] \\
B_{\text{au\_f2}} = \dfrac{U_{\text{dc}}I_{\text{m}}}{4}[k_2\sin\varphi_2+\dfrac{1}{4}m\cos\varphi_1-\dfrac{\sqrt{3}}{12}m\sin\varphi_1]
\end{cases} \quad .(13)$$

Since the derivation processes of phases B and C are similar to that of phase A, this part is put into the Appendix. The amplitudes of $P_{\text{xu\_f1}}$ and $P_{\text{xu\_f2}}$ ($x=a, b, c$) can be obtained using the following equation:

$$\begin{cases} \left| P_{\text{xu\_f1}} \right| = \sqrt{A_{\text{xu\_f1}}{}^2 + B_{\text{xu\_f1}}{}^2} \\ \left| P_{\text{xu\_f2}} \right| = \sqrt{A_{\text{xu\_f2}}{}^2 + B_{\text{xu\_f2}}{}^2} \end{cases} . \tag{14}$$

B. Parameter Determination Method of the Proposed Injection Strategy

According to the previous analysis, the behaviors of arm power fluctuation of the three phases are different from each other. For the SLG fault in phase *A*, the power fluctuation of phase *C* remains constant as pre-fault. However, the power fluctuations of phases *A* and *B* are quite different from the pre-fault state. It can be seen from (11)-(14) that the factors that affect the amplitudes of power fluctuation include the power factor angle φ_1, modulation ratio m, second-harmonic injection coefficient k_2 and initial phase angle of second-harmonic circulating current φ_2. Therefore, the objective function to minimize the three-phase power fluctuation can be defined as:

$$\min P_f(\varphi_1, m, k_2, \varphi_2) = P_{f1}(\varphi_1, m, k_2, \varphi_2) + P_{f2}(\varphi_1, m, k_2, \varphi_2)$$

$$s.t. \tag{15}$$

$$\begin{cases} P_{f1}(\varphi_1, m, k_2, \varphi_2) = \left| P_{\text{au\_f1}} \right| + \left| P_{\text{bu\_f1}} \right| + \left| P_{\text{cu\_f1}} \right| \\ P_{f2}(\varphi_1, m, k_2, \varphi_2) = \left| P_{\text{au\_f2}} \right| + \left| P_{\text{bu\_f2}} \right| + \left| P_{\text{cu\_f2}} \right| \end{cases}$$

In order to ensure that the power fluctuation with the proposed strategy is less than that without the proposed strategy, the following inequality constraint should be satisfied:

$$\begin{cases} P_{f1}(\varphi_1, m, k_2, \varphi_2) \leq P_{f1}(\varphi_1, m, 0, 0) \\ P_{f2}(\varphi_1, m, k_2, \varphi_2) \leq P_{f2}(\varphi_1, m, 0, 0) \end{cases} . \tag{16}$$

In order to avoid the significant increase of the maximum arm current after activating the second harmonic injection, the second harmonic injection coefficient should meet:

$$|k2| \leq 1. \tag{17}$$

The optimal process of the proposed method is shown in Fig. 4. First, the system parameters will be uploaded, and the initial value and traversal step of each variable will be determined. Considering that a dynamic adjustment of m may occur during operation, the optimal process can be divided into two modes. One mode can optimize k_2 and φ_2 to minimize the objective function when φ_1 and m are fixed, which can obtain a local optimum. The other one can optimize m, k_2 and φ_2 to minimize the objective function. The selection of the mode depends on the user demands. Dynamic adjustment of m can be realized by adjusting the DC voltage, which will affect the amplitude of power fluctuation. According to (11)-(14), increasing the modulation ratio dynamically, which means reducing the DC voltage, is helpful to reduce the amplitude of power fluctuation. Therefore, the optimal modulation ratio needs to be greater than the modulation ratio m_{ori} in steady states.
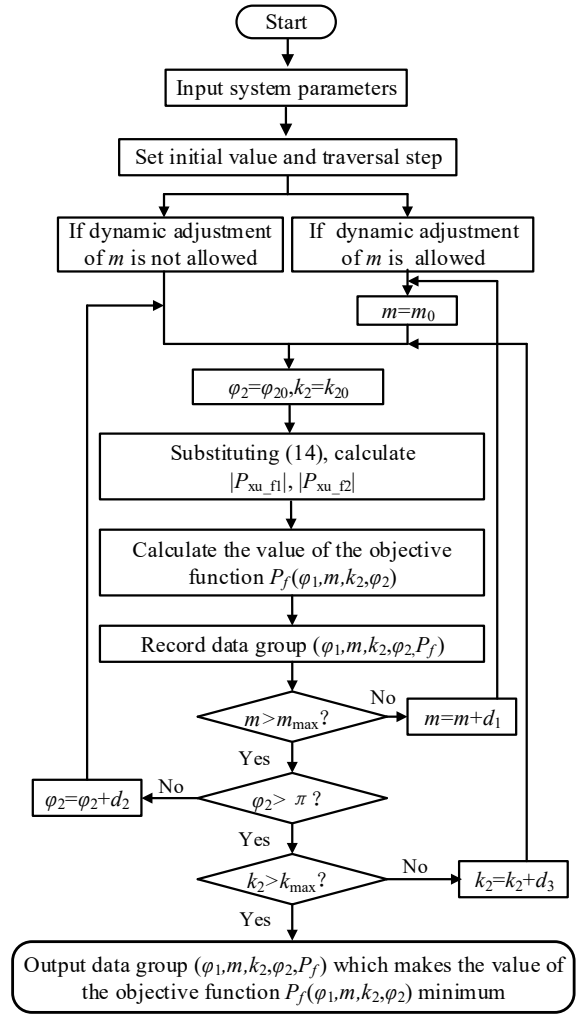

Fig. 4. Flow chart of the optimal process.

Supposing $m \in [m_{\text{ori}}, 3]$, $\varphi_2 \in [-\pi, \pi]$, $k_2 \in [-3,3]$, m_0, φ_{20} and k_{20} are the initial values of m, φ_2 and k_2 ($m_0 = m_{\text{ori}}$, $\varphi_{20} = -\pi$, $k_{20} = -3$). d_1, d_2 and d_3 are the corresponding traversal steps. Then, the variables are inserted to (14) to calculate the amplitude of the fundamental frequency power fluctuation and second-harmonic power fluctuation of each phase, i.e., $|P_{\text{xu\_f1}}|$ and $|P_{\text{xu\_f2}}|$ ($x=a$, b, c). $|P_{\text{xu\_f1}}|$ and $|P_{\text{xu\_f2}}|$ are used to calculate the value of objective function P_f which is recorded with corresponding parameters as a data group (φ_1, m, $k2$, φ_2, P_f). Then the values of φ_2, m and k_2 will be updated and the producers will keep repeating until each parameter reaches their maximum. Finally, the optimal parameters can be obtained by finding the data group with the minimum objective function value.

It should be mentioned that the proposed optimal process is an offline process. The proposed strategy can obtain the appropriate optimal harmonic injection parameters for all operating conditions. Generally, the steady-state operation condition of the converter station is known. According to the steady-state modulation ratio and power factor, the amplitude and phase of the second harmonic needed to be injected after the fault can be calculated in advance and embedded in the control system. Upon an SLG fault, the proposed strategy can be put into operation immediately after fault detection. [28]

proposed an SLG fault detection method which takes 10 ms to detect SLG faults.

To clearly show the performance of the proposed strategy, the arm power fluctuation calculated based on (10) with m=1 and $\cos\varphi_1$=1 is illustrated in Fig. 5. The power fluctuation is in per unit under a base of $U_{dc}I_m/4$. It can be seen that the three-phase arm power fluctuations are effectively reduced with the proposed strategy.
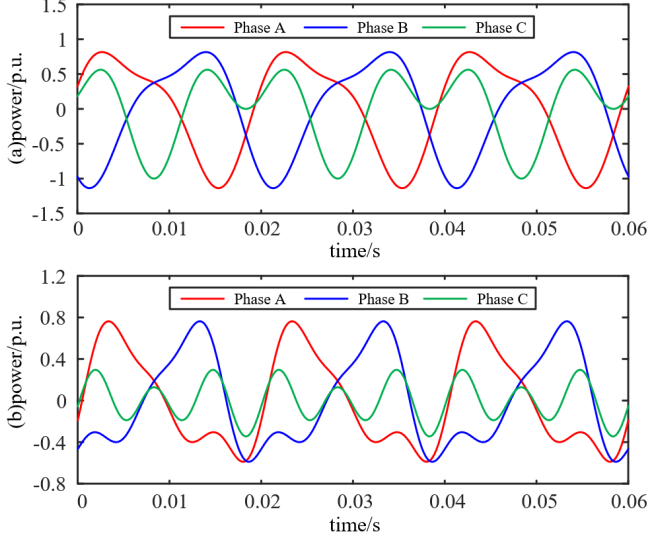

Fig. 5. Arm power fluctuations calculated based on (10) with m=1 and $\cos\varphi_1$=1. (a) the second-harmonic current injection strategy in [19], (b) the proposed strategy.

C. Performance Evaluation

Under steady states, the capacitor voltage fluctuation of the three phases is symmetrical in hybrid MMCs, so the performance of the second-harmonic current injection strategy under steady states can be evaluated by the reduction of the capacitor voltage fluctuation of one phase. The single-phase SM voltage fluctuation mitigation rate (η_j, where j=a, b, c) is defined as:

$$\eta_j = \frac{\Delta U_{jx} - \Delta U_{jy}}{\Delta U_{jx}}, \tag{18}$$

where ΔU_{jx} and ΔU_{jy} are the amplitudes of capacitor voltage fluctuation of phase j without and with the second-harmonic current injection strategy. However, under SLG faults, the three-phase capacitor voltage fluctuations are different from each other. η_j is not enough to evaluate the performance of the second-harmonic current injection strategy under SLG faults. Then, the average voltage fluctuation mitigation rate (η_{ave}) is defined:

$$\eta_{ave} = \frac{\eta_a + \eta_b + \eta_c}{3}. \tag{19}$$
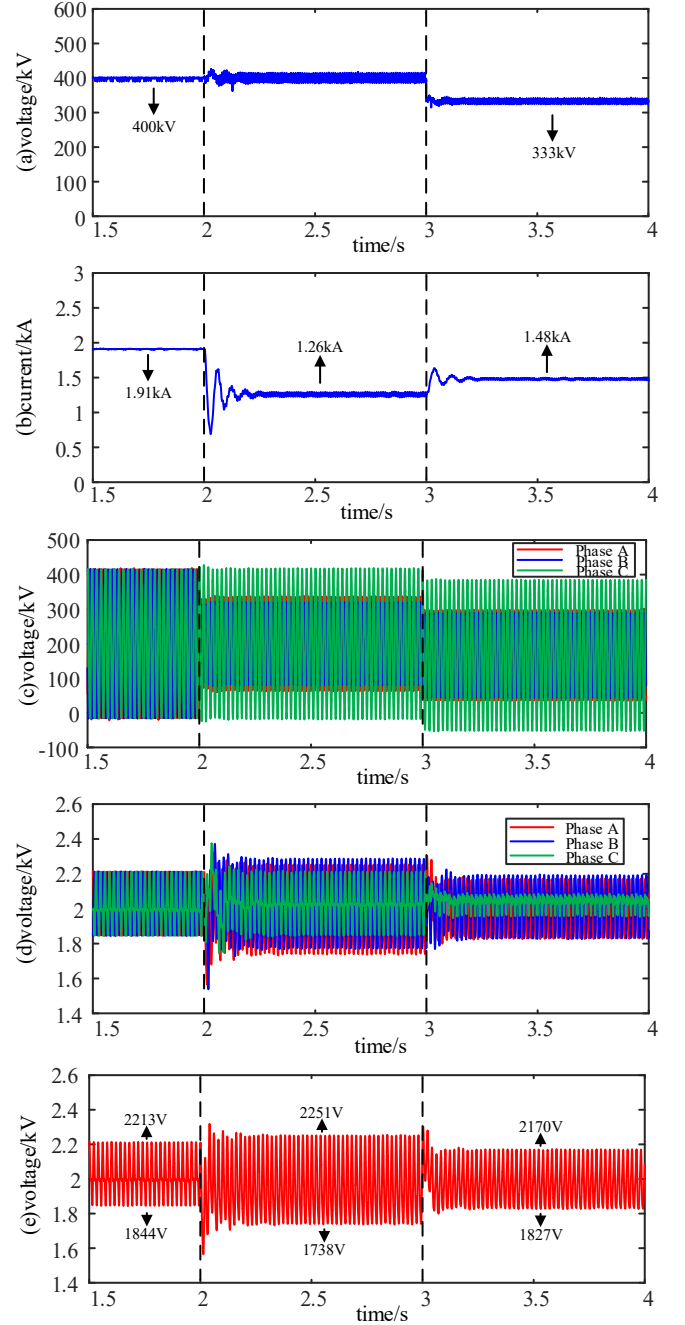
IV. SIMULATION RESULTS

In order to verify the effectiveness of the proposed optimal second-harmonic current injection strategy, a hybrid MMC simulation model has been developed in PSCAD/EMTDC. System parameters of the hybrid MMC are provided in Table I.

TABLE I
PARAMETERS OF THE SIMULATION MODEL

Items	Values
DC voltage	400 kV
Grid-side voltage (rms)	380 kV
Arm reactor	0.056 H
Leakage inductance	0.1 p.u.
Converter capacity	800 MW
Number of FB-SMs per arm	188
Number of HB-SMs per arm	80
Capacitance of SM	5100 μF
Capacitor voltage reference	2 kV

A. Operation Under Unit Power Factor Conditions

Fig. 6 presents the simulation results of hybrid MMC with the proposed strategy under the unit power factor condition.
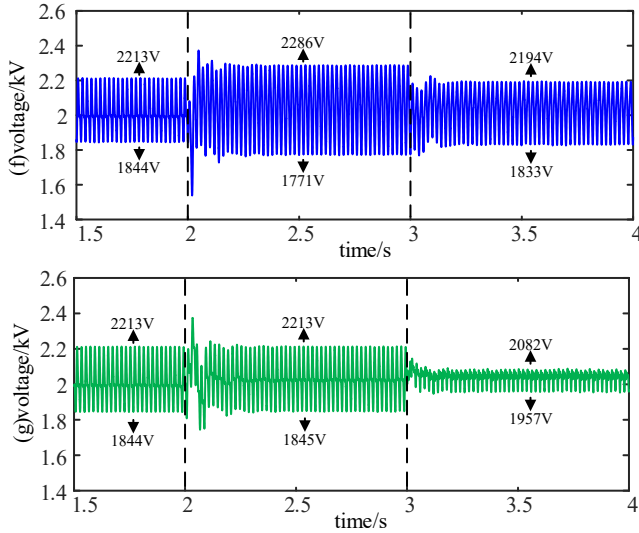
Fig. 6. Simulation results with the proposed strategy under unit power factor condition. (a) DC voltage, (b) DC current, (c) AC voltage, (d) three-phase capacitor voltage, (e) capacitor voltage of phase A, (f) capacitor voltage of phase B, (g) capacitor voltage of phase C.

Before t=2.0 s, the system is in a steady state with m=1 and $\cos\varphi_1$=1. The SLG fault in phase A occurs at t=2.0 s. Then, the proposed second-harmonic current injection strategy is implemented with m=1.2, k_2=0.47 and φ_2=-90° at t=3.0 s. According to Fig. 5 (a), the DC voltage reduced from 400 kV to 333 kV, when the proposed strategy is applied. Fig. 5 (b) shows that the DC current decreases to 1.26 kA when the fault occurs, while it increases to 1.48 kA with the proposed strategy. The three-phase capacitor voltages are presented in Figs. 5 (d)-(g). It can be calculated that the voltage fluctuation mitigation rates of phases A, B, and C are 33.14%, 29.9% and 66%. According to (19), the average voltage fluctuation mitigation rate is 43%. It is seen that the reduction of voltage fluctuation of phase C is the most. It can be concluded based on the obtained results that our scheme can effectively mitigate the capacitor voltage fluctuation under grid-side SLG faults.

B. Impact of Modulation Ratio

To study the impact of the modulation ratio m_{ori} in steady states on the proposed strategy, m_{ori}=0.8 and m_{ori}=1.3 are selected for simulations with $\cos\varphi_1$=1. The parameters optimized by the proposed strategy are m=1.2, k_2=0.47 and φ_2=-90° with m_{ori}=0.8 and that are m=1.3, k_2=0.44 and φ_2=-90° with m_{ori}=1.3. Simulation results of hybrid MMC with different m_{ori} are shown in Fig. 7.
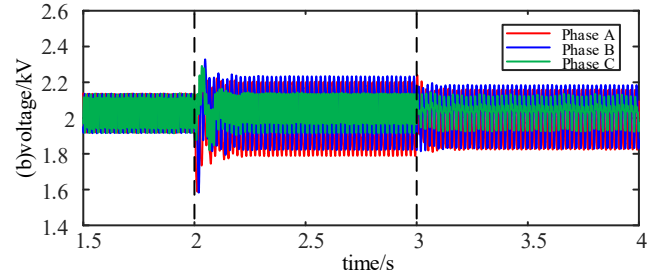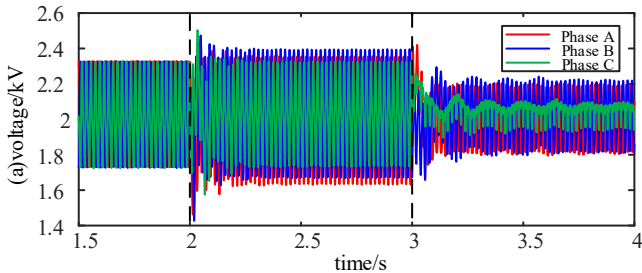

Fig. 7. Simulation results with different m_{ori}. (a) m_{ori}=0.8, (b) m_{ori}=1.3.

It is observed from Figs. 6 and 7 that the amplitude of voltage fluctuation decreases with the increase of m_{ori}. To quantify the impact of m_{ori}, the voltage fluctuation mitigation under different m_{ori} are investigated. The obtained results are listed in Table II.

TABLE II
VOLTAGE FLUCTUATION MITIGATION UNDER DIFFERENT m_{ori}

m_{ori}	Voltage fluctuation mitigation ratios			
	η_a	η_b	η_c	η_{ave}
0.8	47.7%	44.54%	75.12%	55.77%
1	33.14%	29.9%	66%	43%
1.3	21.74%	13.14%	13.24%	16.04%

It can be concluded that the proposed strategy can effectively reduce the capacitor voltage fluctuation with different m_{ori}. The smaller the modulation ratio in steady states is, the greater the average voltage fluctuation reduction rate is. The average voltage fluctuation reduction rate is 55.77% when m_{ori} is 0.8, which is close to 3.5 times of that when m_{ori} is 1.3.

C. Impact of Power Factor

To investigate the impact of the power factor on the proposed strategy, two operating conditions are considered with m_{ori}=1: $\cos\varphi_1$=0.9 and $\cos\varphi_1$=0.8. The parameters optimized by the proposed strategy are m=1.3, k_2=-0.53 and φ_2=57.78° with $\cos\varphi_1$=0.9 and m=1.4, k_2=0.57 and φ_2=-134.74° with $\cos\varphi_1$=0.8. Simulation results of hybrid MMC with different $\cos\varphi_1$ are shown in Fig. 8.
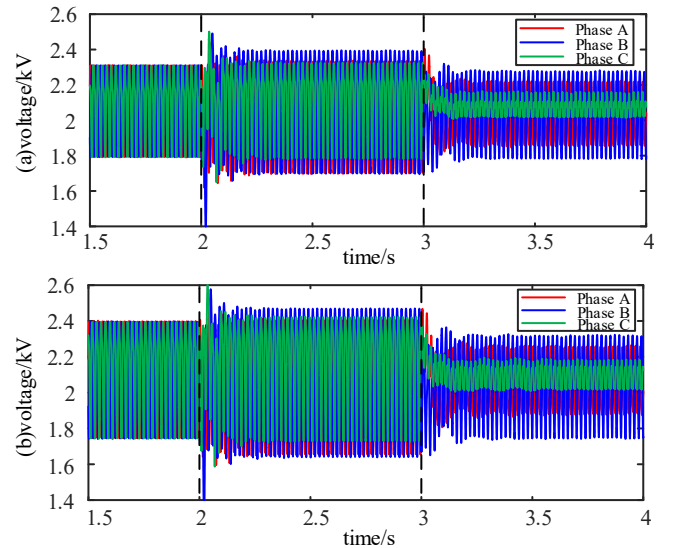

Fig. 8. Simulation results with different $\cos\varphi$. (a) $\cos\varphi_1$=0.9, (b) $\cos\varphi_1$=0.8.

Figs. 6 and 8 show that the amplitude of voltage fluctuation is inversely proportional to $\cos\varphi_1$. It can be seen that when the

power factor decreases, the reactive power will increase, which will lead to the increase of voltage fluctuation. To quantify the impact of $\cos\varphi_1$, the voltage fluctuation mitigation results under different $\cos\varphi_1$ are investigated. The obtained results are listed in Table III.

According to Table III, the power factor does not affect the effectiveness of the proposed strategy. Among the three operating conditions, the proposed strategy with $\cos\varphi_1=0.8$ has the best performance in restraining voltage fluctuation, as η_{ave} reaches 52.07%.

TABLE III
VOLTAGE FLUCTUATION MITIGATION UNDER DIFFERENT $\cos\varphi_1$

$\cos\varphi_1$	Voltage fluctuation mitigation ratios			
	η_a	η_b	η_c	η_{ave}
1	33.14%	29.9%	66%	43%
0.9	42.56%	28.88%	73.7%	48.38%
0.8	49.53%	30.69%	76%	52.07%

D. Verification of Arm Power Fluctuation Model

In order to verify the effectiveness of the proposed arm power fluctuation model under grid-side SLG faults, results of simulation and calculation under a grid-side SLG fault are shown in Fig. 9.
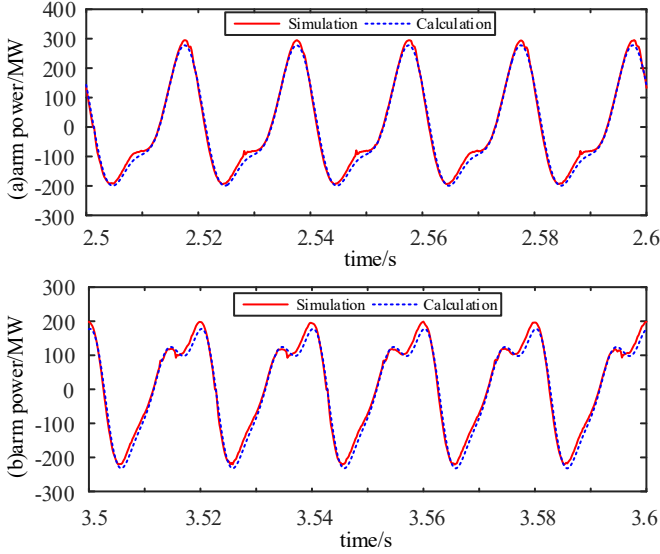

Fig. 9. Results of simulation and calculation under a grid-side SLG fault (m=1, $\cos\varphi_1$=1). (a) Arm power fluctuation without the proposed strategy, (b) Arm power fluctuation with the proposed strategy.

It is observed from Fig. 9 that whether the proposed strategy is put into operation or not, the proposed arm power model shows a good agreement with the simulation results. The results show that the proposed model can well characterize the arm power fluctuation characteristics during the fault.

E. Comparison of Steady-State Strategy and the Proposed Strategy

A dual harmonic current injection strategy for reducing the SM voltage fluctuation in hybrid MMCs has been proposed in [26]. However, it aims to mitigate the SM voltage fluctuation under the steady-state operation. In order to compare strategy in [26] with the proposed strategy. Simulation results of the

strategy in [26] and the proposed strategy after an SLG fault occurs in phase A are given in Fig. 10.
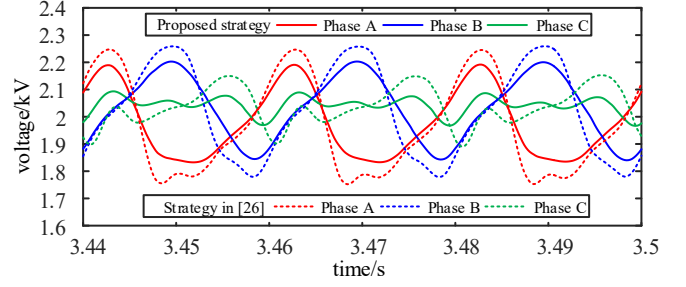

Fig. 10. Capacitor voltage fluctuation under the control strategies in [26] and our paper.

The simulation conditions in Fig. 10 are the same as those in Fig. 6. It can be calculated that the voltage fluctuation mitigation rates of phases A, B, and C with the strategy in [26] are 4.09%, 6.8% and 32.34%, while the proposed strategy achieves 33.14%, 29.9% and 66%. Simulation results show that the strategy in [26] performs less effective in suppressing the capacitor voltage fluctuation under grid-side SLG faults compared to the proposed strategy in this paper.

V. CONCLUSION

In this paper, the mathematical models of arm power fluctuations of MMC have been developed under steady states and grid-side SLG faults. It has been proved that the second-harmonic current injection strategy used for steady states will increase capacitor voltage fluctuation under grid-side SLG faults. Based on the theoretical analysis, an optimal second-harmonic current injection strategy is proposed for capacitor voltage fluctuation reduction in hybrid MMCs under grid-side SLG faults. With the proposed strategy, the three-phase power fluctuation under grid-side SLG faults can be reduced by optimizing the modulation ratio, second-harmonic injection coefficient and initial phase angle of the second-harmonic circulating current. In this case, the capacitor voltage fluctuation can be reduced at the same time. Simulation results show that the average voltage fluctuation mitigation rate can be 55.77% if the proposed strategy is applied. Moreover, it is concluded that the modulation ratio in steady states and the power factor do not affect the effectiveness of the proposed strategy.

REFERENCES

[1] G. Li, J. Liang, F. Ma, C. E. Ugalde-Loo and H. Liang, "Analysis of Single-Phase-to-Ground Faults at the Valve Side of HB-MMC in HVDC Converter Stations," *IEEE Trans. Ind. Electron.*, vol. 66, no. 3, pp. 2444-2453, March 2019.

[2] A. Nami, J. Liang, F. Dijkhuizen, and G. D. Demetriades, "Modular multilevel converters for HVDC applications: Review on converter cells and functionalities," *IEEE Trans. Power Electron.*, vol. 30, no. 1, pp. 18–36, Jan. 2015.

[3] G. Li et al., "Feasibility and reliability analysis of LCC DC grids and LCC/VSC hybrid DC grids," *IEEE Access*, vol. 7, pp. 22445–22456, 2019.

[4] G. Li et al., "Power reversal strategies for hybrid LCC/MMC HVDC systems," *CSEE Journal of Power and Energy Systems*, vol. 6, no. 1, pp. 203-212, March 2020.

[5] M. M. C. Merlin and T. C. Green, "Cell capacitor sizing in multilevel converters: cases of the modular multilevel converter and alternate arm converter," *IET Power Electron.*, vol. 8, no. 3, pp. 350-360, Jan. 2015.

[6] C. Zhao et al., "Energy Storage Requirements Optimization of Full-Bridge MMC With Third-Order Harmonic Voltage Injection," *IEEE Trans. Power Electron.*, vol. 34, no. 12, pp. 11661-11678, Dec. 2019.

[7] J. Pou et al., "Circulating current injection methods based on instantaneous information for the modular multilevel converter," *IEEE Trans. Ind. Electron.*, vol. 62, no. 2, pp. 777–788, Feb. 2015.

[8] R. Picas et al., "Minimization of the capacitor voltage fluctuations of a modular multilevel converter by circulating current control," *in Proc. IEEE Energy Convers. Congr. Expo.*, 2011, pp. 4985–4991.

[9] R. Picas et al., "Optimal injection of harmonics in circulating currents of modular multilevel converters for capacitor voltage ripple minimization," *in Proc. IEEE ECCE Asia Downunder Conf.*, 2013. pp. 318–324.

[10] A. J. Korn, M. Winkelnkemper and P. Steimer, "Low output frequency operation of the modular multi-level converter," *in Proc. IEEE ECCE*, Atlanta, GA, USA, Sep. 12-16, 2010, pp. 3993-3997.

[11] K. Ilves, S. Norrga, L. Harnefors, and H. P. Nee, "On energy storage requirements in modular multilevel converters," *IEEE Trans. Power Electron.*, vol. 29, no. 1, pp. 77–88, Jan. 2014.

[12] R. Li, J. E. Fletcher and B. W. Williams, "Influence of third harmonic injection on modular multilevel converter-based high-voltage direct current transmission systems," *IET Gen. Trans. Distrib.*, vol. 10, no. 11, pp. 2764-2770, July. 2016.

[13] X. Yu, Y. Wei, Q. Jiang, X. Xie, Y. Liu, and K. Wang, "A novel hybrid arm bipolar MMC topology with dc fault ride-through capability," *IEEE Trans. Power Del.*, vol. 32, no. 3, pp. 1404–1413, May 2017.

[14] J. Hu, K. Xu, L. Lin, and R. Zeng, "Analysis and enhanced control of hybrid-MMC-based HVDC systems during asymmetrical DC voltage faults," *IEEE Trans. Power Del.*, vol. 32, no. 3, pp. 1394–1403, Jun. 2017.

[15] R. Zeng, L. Xu, L. Yao, and B. W. Williams, "Design and operation of a hybrid modular multilevel converter," *IEEE Trans. Power Electron.*, vol. 30, no. 3, pp. 1137–1146, Mar. 2015.

[16] R. Zeng, L. Xu, L. Yao, and D. John Morrow, "Precharging and DC fault ride-through of hybrid MMC-based HVDC systems," *IEEE Trans. Power Del.*, vol. 30, no. 3, pp. 1298–1306, Jun. 2015.

[17] J. Xu, P. Zhao and C. Zhao, "Reliability Analysis and Redundancy Configuration of MMC With Hybrid Submodule Topologies," *IEEE Trans. Power Electron.*, vol. 31, no. 4, pp. 2720-2729, April 2016.

[18] J. Jung, S. Cui, J. Lee and S. Sul, "A New Topology of Multilevel VSC Converter for a Hybrid HVDC Transmission System," *IEEE Trans. Power Electron.*, vol. 32, no. 6, pp. 4199-4209, June 2017.

[19] C. Zhao et al., "Energy Storage Requirement Optimization of Hybrid Modular Multilevel Converter With Circulating Current Injection," *IEEE Trans. Ind. Electron*, vol. 66, no. 9, pp. 6637-6648, Sept. 2019.

[20] J. Hu, M. Xiang, L. Lin, M. Lu, J. Zhu and Z. He, "Improved design and control of FBSM MMC with boosted AC voltage and reduced DC capacitance," *IEEE Trans. Ind. Electron.*, vol. 65, no. 3, pp. 1919–1930, Mar. 2018.

[21] M. Lu, J. Hu, R. Zeng, W. Li, and L. Lin, "Imbalance mechanism and balanced control of capacitor voltage for a hybrid modular multilevel converter," *IEEE Trans. Power Electron.*, vol. 33, no. 7, pp. 5686–5696, Jul. 2018.

[22] M. Lu, J. Hu, R. Zeng, and Z. He, "Fundamental-frequency reactive circulating current injection for capacitor voltage balancing in Hybrid-MMC HVDC systems during riding through PTG faults," *IEEE Trans. Power Del.*, vol. 33, no. 3, pp. 1348–1357, Jun. 2018.

[23] T. Bandaru, D. Samajdar, P. B. S. Varma, T. Bhattacharya and D. Chatterjee, "Optimum Injection of Second Harmonic Circulating Currents for Balancing Capacitor Voltages in Hybrid MMC during Reduced DC Voltage Conditions," *IEEE Trans. Ind. Appl.*, vol. 56, no. 2, pp. 1649-1660, March-April 2020.

[24] M. Guan and Z. Xu, "Modeling and control of a modular multilevel converter-based HVDC system under unbalanced grid conditions," *IEEE Trans. Power Electron.*, vol. 27, no. 12, pp. 4858–4867, Dec. 2012.

[25] C. Zhao, F. Gao, Z. Li, P. Wang and Y. Li, "Modulation Index Design of Full-Bridge MMC for Capacitor Voltage Ripples Reduction Under Single-Line-to-Ground Faults Conditions," *IEEE Trans. Power Del.*, Aug. 2020. (Early Access)

[26] J. Xu et al., "Dual Harmonic Injection for Reducing the Sub-module Capacitor Voltage Ripples of Hybrid MMC," *IEEE Trans. Emerg. Sel. Topics Power Electron.*, Sep. 2020. (Early Access)

[27] X. Shi, Z. Wang, B. Liu, Y. Li, L. M. Tolbert and F. Wang, "Steady-State Modeling of Modular Multilevel Converter Under Unbalanced Grid Conditions," *IEEE Trans. Power Electron*, vol. 32, no. 9, pp. 7306-7324, Sept. 2017.

[28] J. Chen, H. Li, C. Deng and G. Wang, "Detection of Single-Phase to Ground Faults in Low-Resistance Grounded MV Systems," *IEEE Trans. Power Del.*, vol. 36, no. 3, pp. 1499-1508, June 2021.

APPENDIX

From equation (10), the fundamental-frequency and second-harmonic components $P_{\text{bu\_f1}}$ and $P_{\text{bu\_f2}}$ of the upper arm power fluctuation in phase B can be obtained:

$$
\begin{cases}
P_{\text{bu\_f1}} = \dfrac{U_{\text{dc}}I_{\text{m}}}{4}[-\dfrac{1}{3}(\dfrac{1}{2}-\dfrac{\sqrt{3}}{6}\tan\varphi_1)m^2\cos\varphi_1\sin(\omega t-\dfrac{2}{3}\pi) \\
\quad -\dfrac{1}{6}(\dfrac{1}{2}-\dfrac{\sqrt{3}}{6}\tan\varphi_1)m^2\cos\varphi_1\sin\omega t-\dfrac{1}{3}k_2 m\cos(\omega t+\varphi_2-\dfrac{2}{3}\pi) \\
\quad -\dfrac{1}{6}mk_2\cos(\omega t+\varphi_2+\dfrac{2}{3}\pi)+\sin(\omega t-\varphi_1-\dfrac{2}{3}\pi)] \\
P_{\text{bu\_f2}} = \dfrac{U_{\text{dc}}I_{\text{m}}}{4}[\dfrac{1}{3}m\cos(2\omega t-\varphi_1+\dfrac{2}{3}\pi)+\dfrac{1}{6}m\cos(2\omega t-\varphi_1-\dfrac{2}{3}\pi) \\
\quad +k_2\sin(2\omega t+\varphi_2+\dfrac{2}{3}\pi)]
\end{cases}
$$

Using the trigonometric transformation, $P_{\text{bu\_f1}}$ and $P_{\text{bu\_f2}}$ can be rewritten as:

$$P_{\text{bu\_f1}} = A_{\text{bu\_f1}}\sin\omega t + B_{\text{bu\_f1}}\cos\omega t$$

$$
\begin{cases}
A_{\text{bu\_f1}} = \dfrac{U_{\text{dc}}I_{\text{m}}}{4}[\cos(\varphi_1+\dfrac{2}{3}\pi)+\dfrac{1}{3}mk_2\sin(\varphi_2-\dfrac{2}{3}\pi) \\
\quad +\dfrac{1}{6}mk_2\sin(\varphi_2+\dfrac{2}{3}\pi)] \\
B_{\text{bu\_f1}} = \dfrac{U_{\text{dc}}I_{\text{m}}}{4}[\dfrac{\sqrt{3}}{6}(\dfrac{1}{2}-\dfrac{\sqrt{3}}{6}\tan\varphi_1)m^2\cos\varphi_1-\sin(\varphi_1+\dfrac{2}{3}\pi) \\
\quad -\dfrac{1}{3}mk_2\cos(\varphi_2-\dfrac{2}{3}\pi)-\dfrac{1}{6}mk_2\cos(\varphi_2+\dfrac{2}{3}\pi)]
\end{cases}
,
$$

$$P_{\text{bu\_f2}} = A_{\text{bu\_f2}}\sin 2\omega t + B_{\text{bu\_f2}}\cos 2\omega t$$

$$
\begin{cases}
A_{\text{bu\_f2}} = \dfrac{U_{\text{dc}}I_{\text{m}}}{4}[k_2\cos(\varphi_2+\dfrac{2}{3}\pi)-\dfrac{1}{4}m\sin\varphi_1-\dfrac{\sqrt{3}}{12}m\cos\varphi_1] \\
B_{\text{bu\_f2}} = \dfrac{U_{\text{dc}}I_{\text{m}}}{4}[k_2\sin(\varphi_2+\dfrac{2}{3}\pi)-\dfrac{1}{4}m\cos\varphi_1+\dfrac{\sqrt{3}}{12}m\sin\varphi_1]
\end{cases}
.
$$

From equation (10), the fundamental-frequency and second-harmonic component $P_{\text{cu\_f1}}$ and $P_{\text{cu\_f2}}$ of the upper arm power fluctuation in phase C can be obtained:

$$
\begin{cases}
P_{\text{cu\_f1}} = \dfrac{U_{\text{dc}}I_{\text{m}}}{4}[-\dfrac{1}{2}m^2\cos\varphi_1\sin(\omega t+\dfrac{2}{3}\pi)+\sin(\omega t-\varphi_1+\dfrac{2}{3}\pi) \\
\quad -\dfrac{1}{2}mk_2\cos(\omega t+\varphi_2+\dfrac{2}{3}\pi)] \\
P_{\text{cu\_f2}} = \dfrac{U_{\text{dc}}I_{\text{m}}}{4}[\dfrac{1}{2}m\cos(2\omega t-\varphi_1+\dfrac{4}{3}\pi)+k_2\sin(2\omega t+\varphi_2+\dfrac{4}{3}\pi)]
\end{cases}
.
$$

Using the trigonometric transformation, P_{cu_f1} and P_{cu_f2} can be rewritten as:

$$P_{cu\_f1} = A_{cu\_f1} \sin(\omega t + \frac{2}{3}\pi) + B_{cu\_f1}(\omega t + \frac{2}{3}\pi)$$

$$\begin{cases} A_{cu\_f1} = \dfrac{U_{dc}I_m}{4}[-\dfrac{1}{2}m^2 \cos\varphi_1 + \cos\varphi_1 + \dfrac{1}{2}mk_2 \sin\varphi_2] \\ B_{cu\_f1} = \dfrac{U_{dc}I_m}{4}[-\sin\varphi_1 - \dfrac{1}{2}mk_2 \cos\varphi_2] \end{cases},$$

$$P_{cu\_f2} = A_{cu\_f2} \sin(2\omega t + \frac{4}{3}\pi) + B_{cu\_f2} \cos(2\omega t + \frac{4}{3}\pi)$$

$$\begin{cases} A_{cu\_f2} = \dfrac{U_{dc}I_m}{4}[\dfrac{1}{2}m \sin\varphi_1 + k_2 \cos\varphi_2] \\ B_{cu\_f2} = \dfrac{U_{dc}I_m}{4}[\dfrac{1}{2}m \cos\varphi_1 + k_2 \sin\varphi_2] \end{cases}.$$

Jianzhong Xu (M'14-SM'19) was born in Shanxi, China. He received the B.S. and Ph.D. degrees from North China Electric Power University (NCEPU) in 2009 and 2014 respectively. Currently, he is an Associate Professor and Ph.D. Supervisor of the State Key Laboratory of Alternate Electrical Power System with Renewable Energy Sources, North China Electric Power University, China, where he obtained his Ph.D. degree in 2014. From 2012 to 2013 and 2016 to 2017, he was a visiting Ph.D. student and Post-Doctoral Fellow at the University of Manitoba, Canada. He is an Associate Editor of the CSEE Journal of Power and Energy Systems. He is now working on the Electromagnetic Transient (EMT) equivalent modelling, fault analysis and protection of HVDC Grids.

Weicheng Deng was born in Jiangxi, China. he received the B.S. degree in power system and its automation from North China Electric Power University (NCEPU) in 2019, where he is currently working toward his master degree. His research interests include HVdc grid operation and protection.

Gen Li (M'18) received the B.Eng. degree in Electrical Engineering and its Automation from Northeast Electric Power University, Jilin, China, in 2011, the M.Sc. degree in Power Engineering from Nanyang Technological University, Singapore, in 2013 and the Ph.D. degree in Electrical Engineering from Cardiff University, Cardiff, U.K., in 2018.

From 2013 to 2016, he was a Marie Curie Early Stage Research Fellow funded by the European Commission's MEDOW project. He has been a Visiting Researcher at China Electric Power Research Institute and Global Energy Interconnection Research Institute, Beijing, China, at Elia, Brussels, Belgium and at Toshiba International (Europe), London, U.K. He has been a Research Associate at the School of Engineering, Cardiff University since 2017. His research interests include control and protection of HVDC and MVDC technologies, power electronics, reliability modelling and evaluation of power electronics systems.

Dr. Li is a Chartered Engineer in the U.K. He is an Associate Editor of the CSEE Journal of Power and Energy Systems. He is an Editorial Board Member of CIGRE ELECTRA. He is an IET Professional Registration Advisor. His Ph.D. thesis received the First CIGRE Thesis Award in 2018. He is the Vice-Chair of IEEE PES Young Professionals and Technical Panel Sectary of CIGRE UK B5 Protection and Automation.

Chengyong Zhao (M'05-SM'15) was born in Zhejiang, China. He received the B.S., M.S. and Ph.D. degrees in power system and its automation from NCEPU in 1988, 1993 and 2001, respectively. He was a visiting professor at the University of Manitoba from Jan. 2013 to Apr. 2013 and Sep. 2016 to Oct. 2016. Currently, he is a professor at the School of Electrical and Electronic Engineering, NCEPU. His research interests include HVDC system and DC grid.

Chongru Liu (M'10-SM'15), received her B.S., M.S. and Ph.D. degree in E.E. from Tsinghua University, Beijing, China. She is now a professor, Ph. D. supervisor and the Dean of Academic Affaires Office, North China Electric Power University. Beijing Science and Technology Nova Talent Support Plan was selected in 2009, and the Ministry of Education Excellent Talents Support Plan for the New Century in 2012. Senior member of IEEE, Standing Director of the Tenth Council of Beijing Electrical Engineering Society, Director of the Committee on Science Popularization and Education, Member of the Fifth and Sixth National Technical Committee on Power System Management and Information Exchange Standardization, Member of the Power System Automation Committee of China Electrical Engineering Society, Member of the Foreign Affairs Committee of China Electrical Engineering Society, and Member of Beijing Science Representatives of the Ninth Congress of the Technical Association.